# Porous oxygen vacancy-rich $V_2O_5$ nanosheets as superior semiconducting supports of nonprecious metal nanoparticles for efficient on-demand $H_2$ evolution from ammonia borane under visible light irradiation

Jin Song, Xiaojun Gu,* Yaduo Cao and Hao Zhang

Inner Mongolia Key Laboratory of Coal Chemistry, School of Chemistry and Chemical Engineering, Inner Mongolia University, Hohhot 010021, China

E-mail: xiaojun.gu@yahoo.com

**Calculation method**

The TOF value was calculated from the following equation.

$$\mathrm{TOF} = \frac{3n_{\mathrm{NH3BH3}}}{n_{\mathrm{metal}}t}$$

In the equation, $n_{metal}$ is the total molar amount of metal species in the catalyst, t is reaction time, and $n_{NH3BH3}$ is the total molar amount of $NH_3BH_3$ in the catalytic reaction.

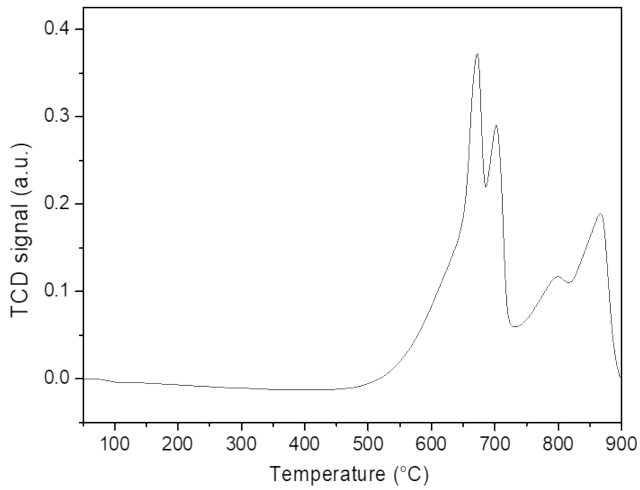


**Fig. S1** $H_2$-TPR profile of pristine $V_2O_5$ in the range of 50–900 °C.

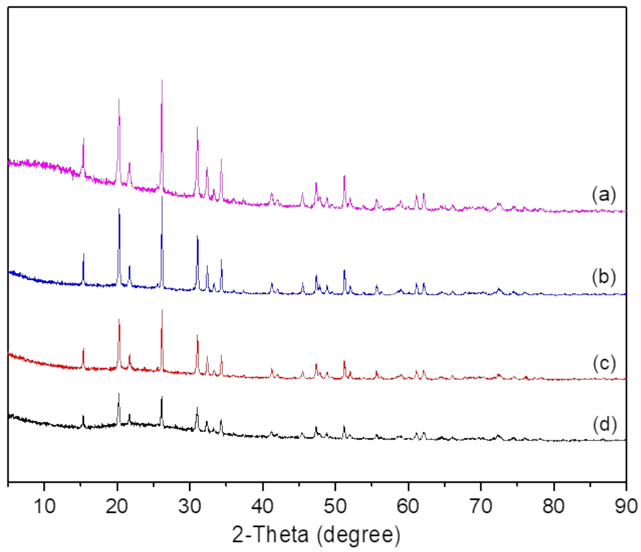


**Fig. S2** PXRD patterns of (a) $V_2O_5$, (b) $V_2O_5$-250, (c) $V_2O_5$-300 and (d) $V_2O_5$-350.

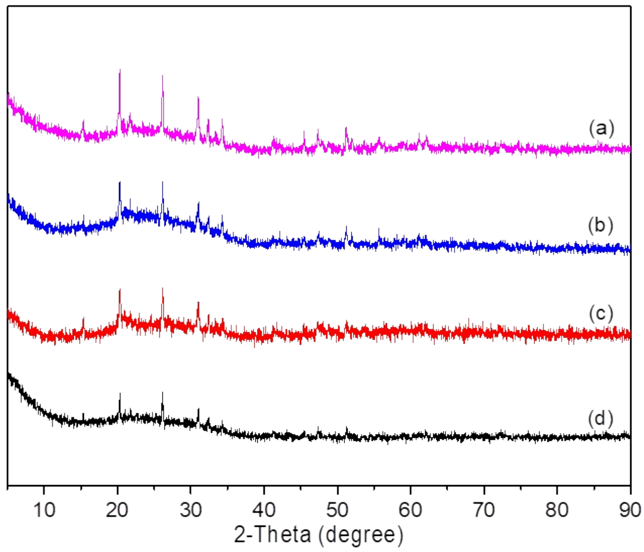


**Fig. S3** PXRD patterns of (a) $Co/V_2O_5$, (b) $Co/V_2O_5$-250, (c) $Co/V_2O_5$-300 and (d) $Co/V_2O_5$-350.

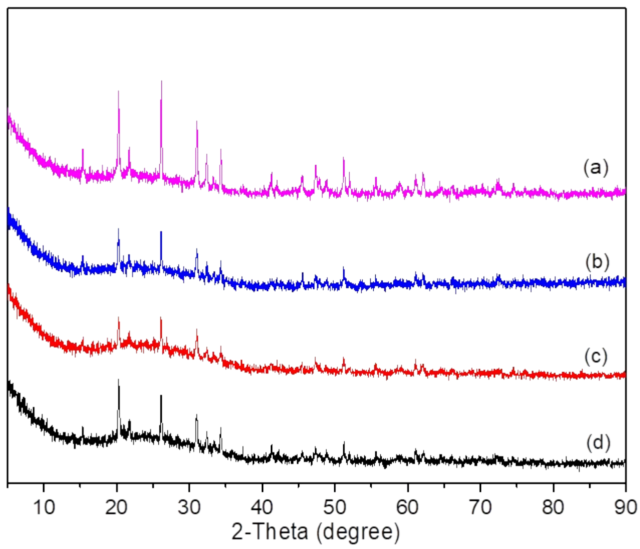


**Fig. S4** PXRD patterns of (a) $Ni/V_2O_5$, (b) $Ni/V_2O_5$-250, (c) $Ni/V_2O_5$-300 and (d) $Ni/V_2O_5$-350.

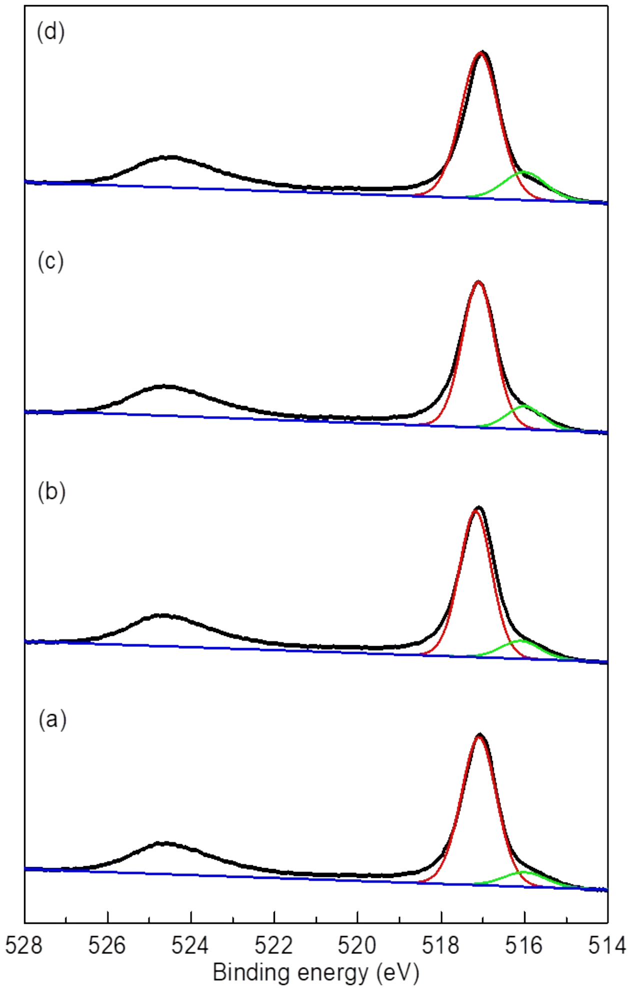


**Fig. S5** XPS patterns of V2p for (a) $V_2O_5$, (b) $V_2O_5$-250, (c) $V_2O_5$-300 and (d) $V_2O_5$-350.

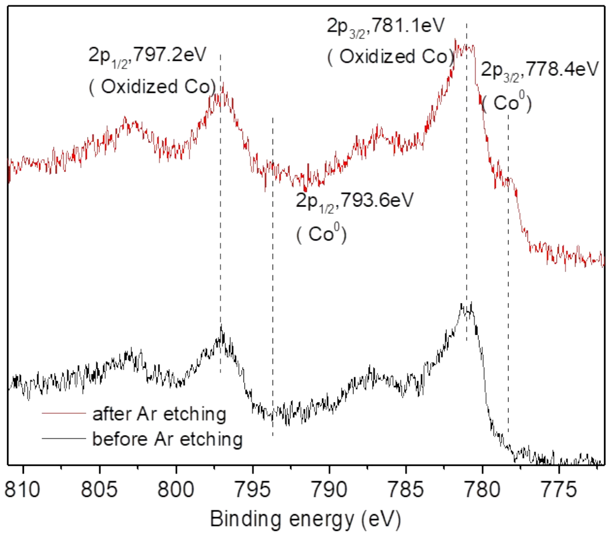


**Fig. S6** XPS patterns of Co 2p in Co/$V_2O_5$-300 before and after Ar etching.

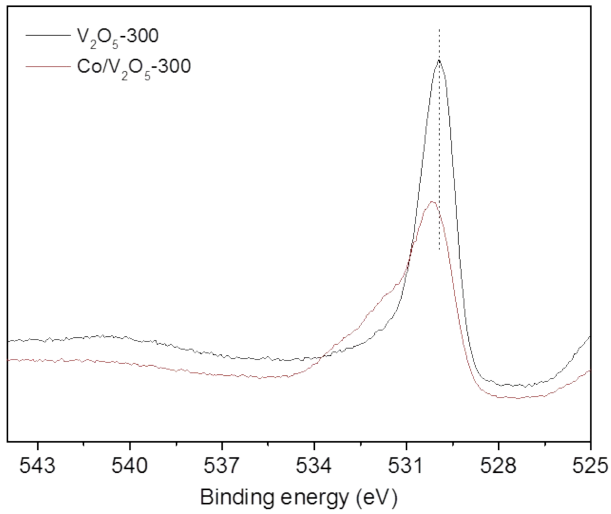


**Fig. S7** XPS patterns of O 1s in $V_2O_5$-300 and Co/$V_2O_5$-300.

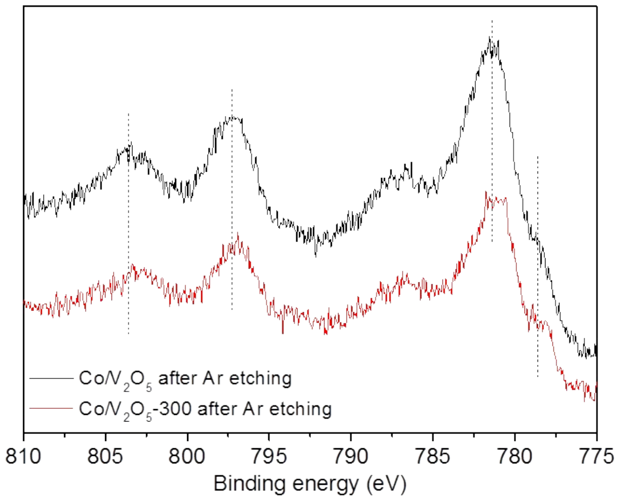


**Fig. S8** XPS patterns of Co 2p in Co/$V_2O_5$ and Co/$V_2O_5$-300.

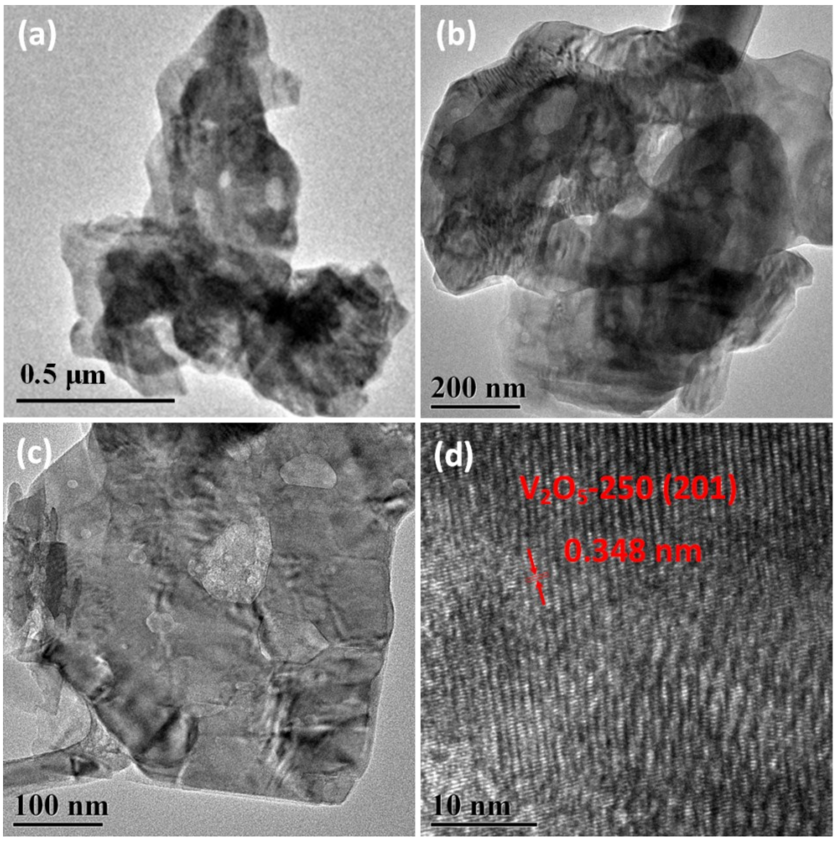


**Fig. S9** TEM images of $V_2O_5$-250 with different magnifications.

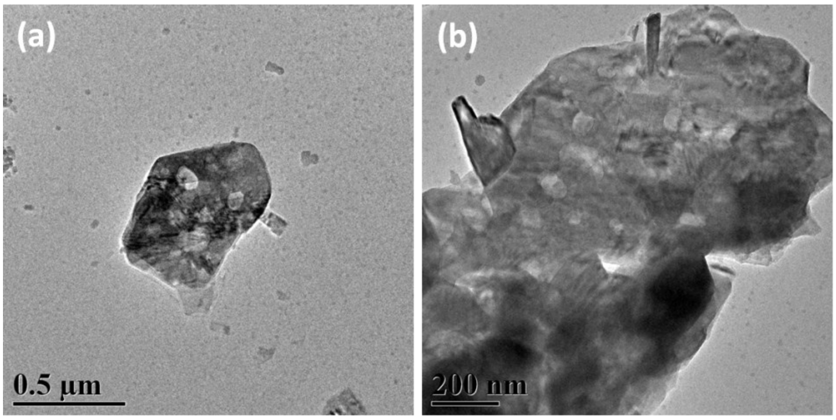


**Fig. S10** TEM images of $V_2O_5$-300 with different magnifications.

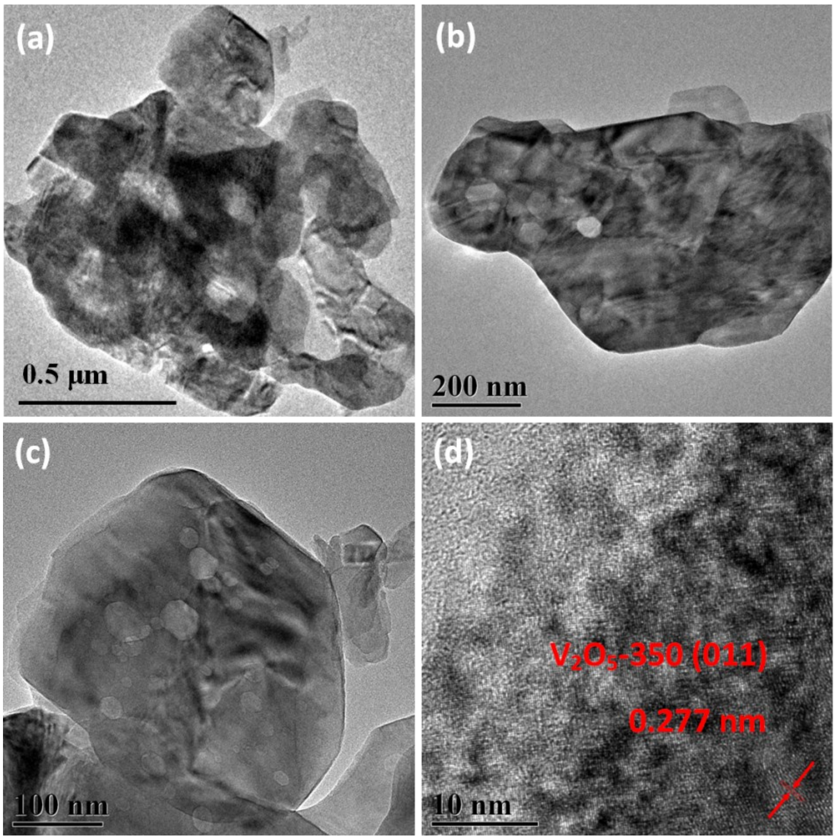


**Fig. S11** TEM images of $V_2O_5$-350 with different magnifications.

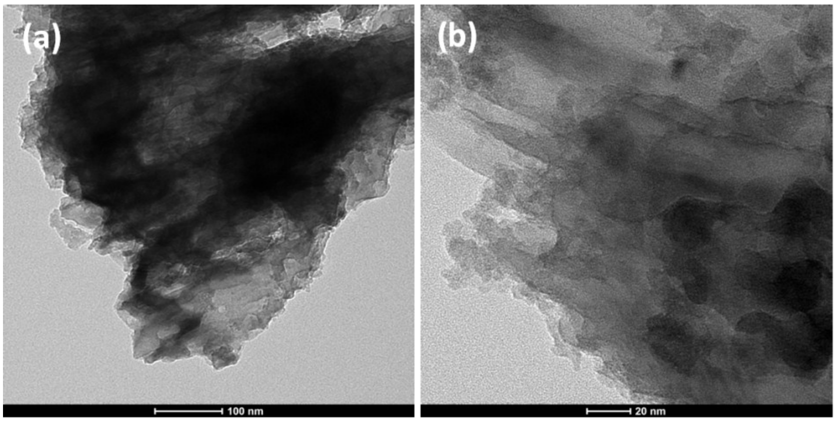


**Fig. S12** TEM images of $Co/V_2O_5$-300.

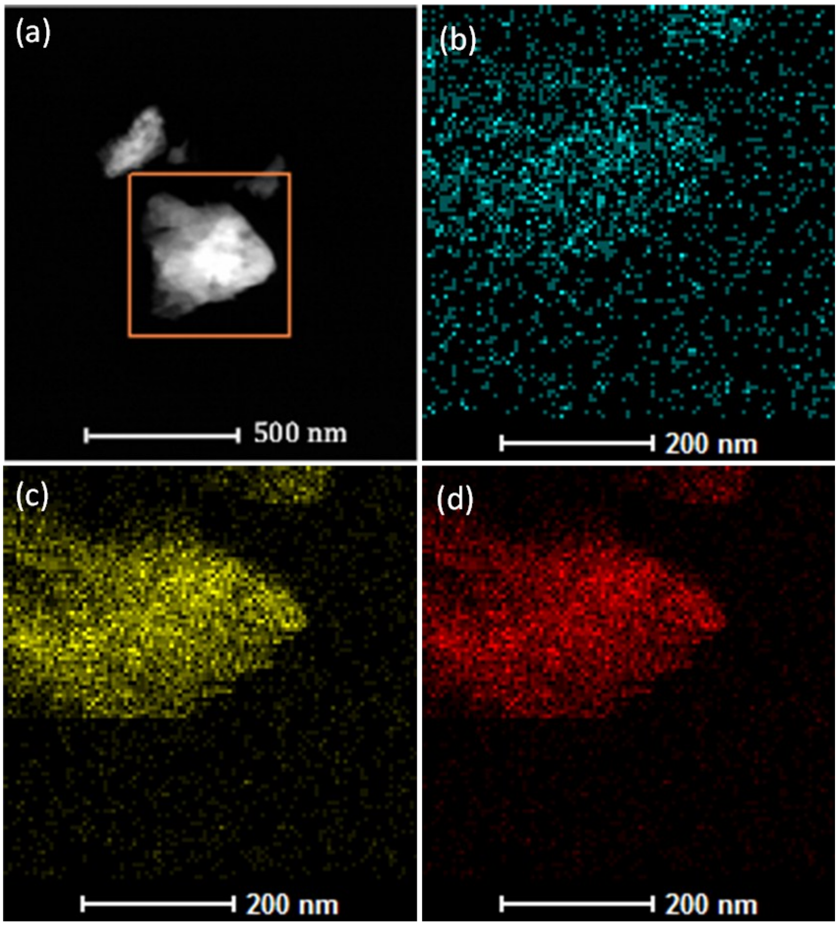


**Fig. S13** HAADF-STEM images of (a) $Co/V_2O_5$-300 and the corresponding elemental maps of $Co/V_2O_5$-300 for (b) Co, (c) V and (d) O.

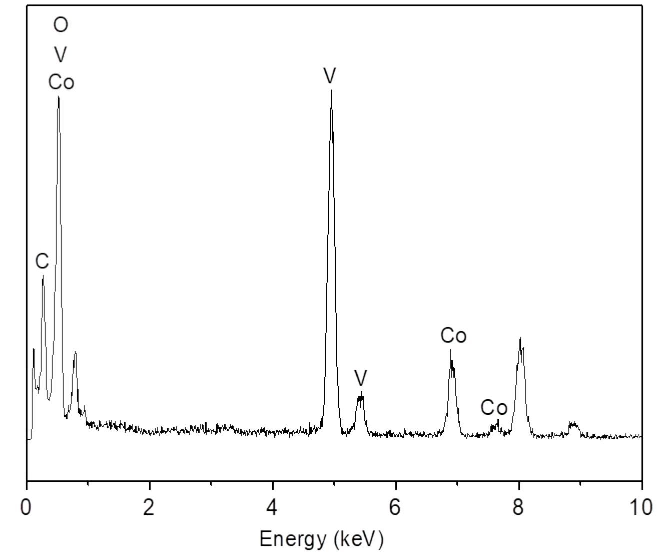


**Fig. S14** EDX pattern of $Co/V_2O_5$.

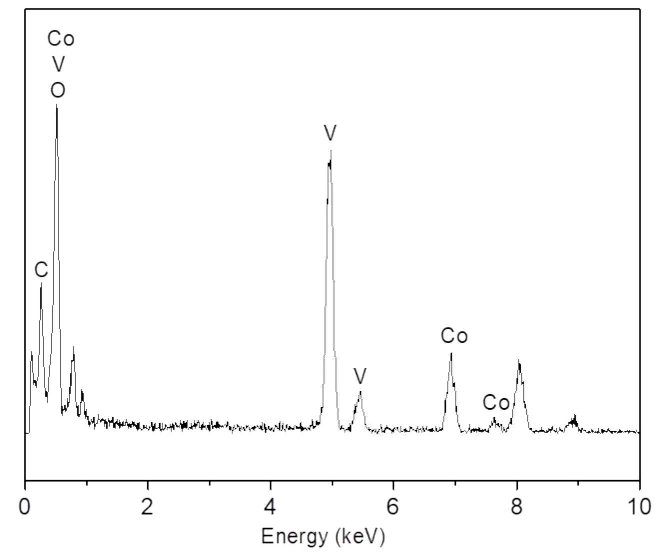


**Fig. S15** EDX pattern of $Co/V_2O_5$-300.

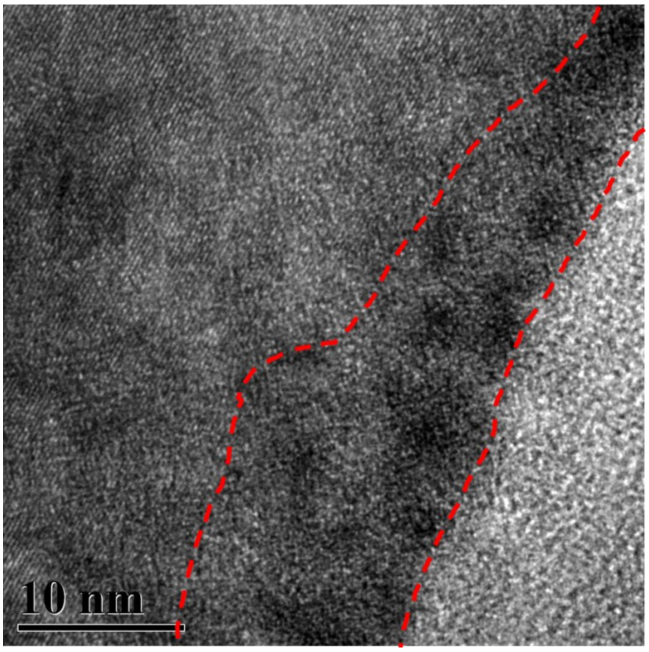


**Fig. S16** TEM image of $Co/V_2O_5$-300.

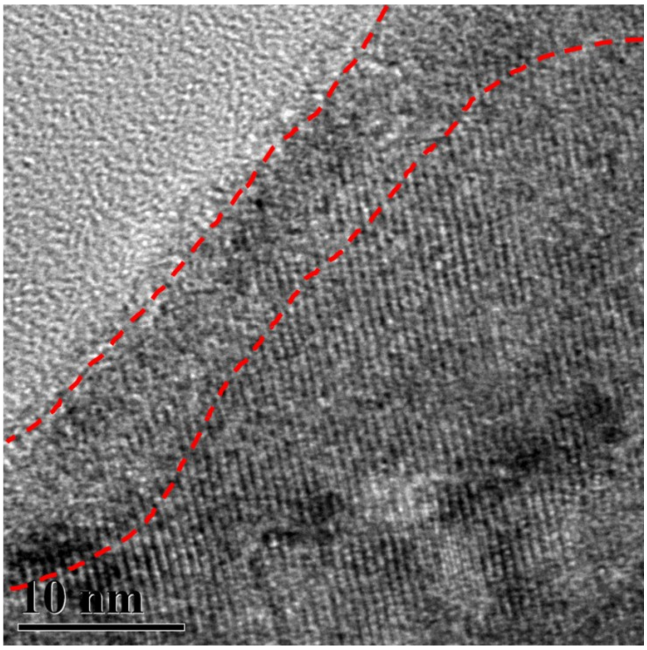


**Fig. S17** TEM image of $Co/V_2O_5$-350.

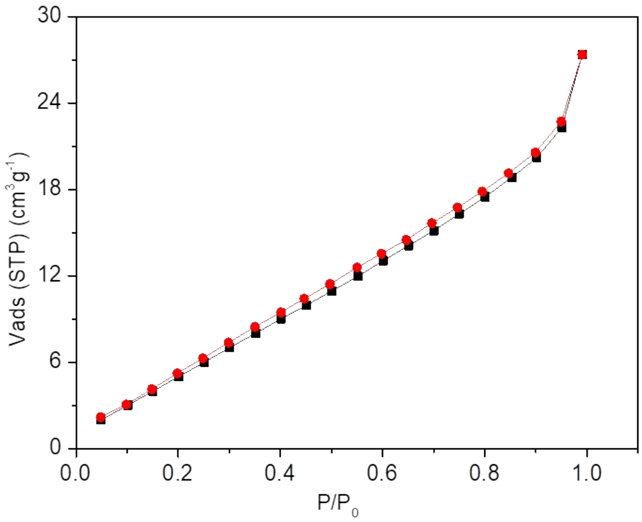


**Fig. S18** $N_2$ adsorption-desorption isotherms of $V_2O_5$ at 77K.

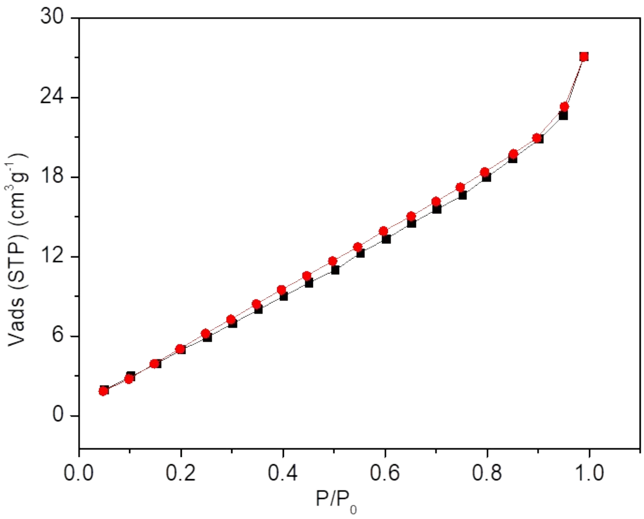


**Fig. S19** $N_2$ adsorption-desorption isotherms of $V_2O_5$-300 at 77K.

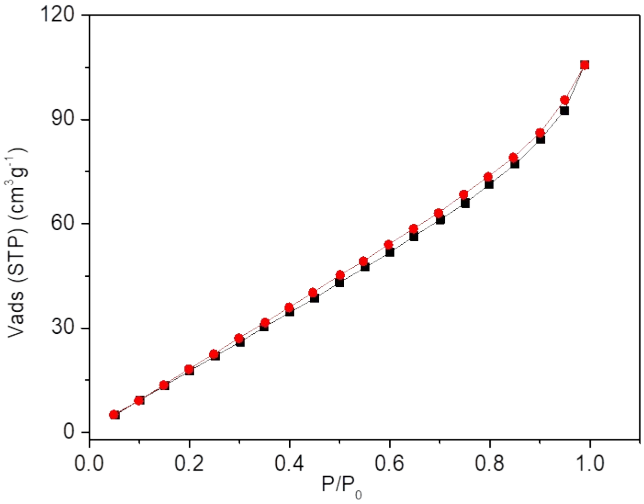


**Fig. S20** $N_2$ adsorption-desorption isotherms of $Co/V_2O_5$ at 77 K.

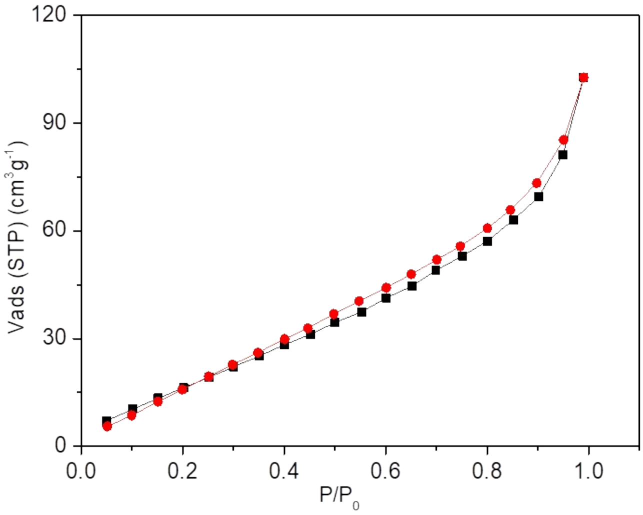


**Fig. S21** $N_2$ adsorption-desorption isotherms of $Co/V_2O_5$-300 at 77K.

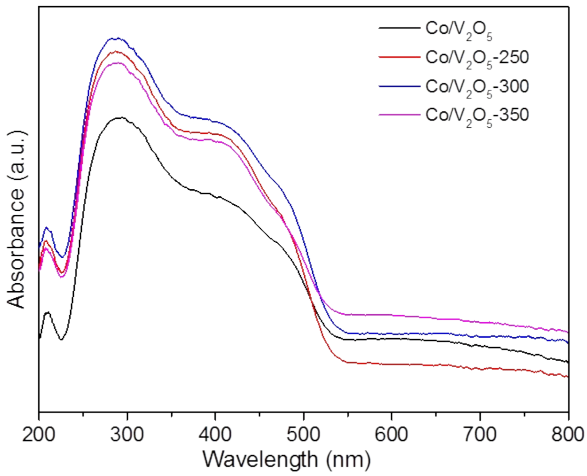


**Fig. S22** UV-vis spectra of four Co-based catalysts.

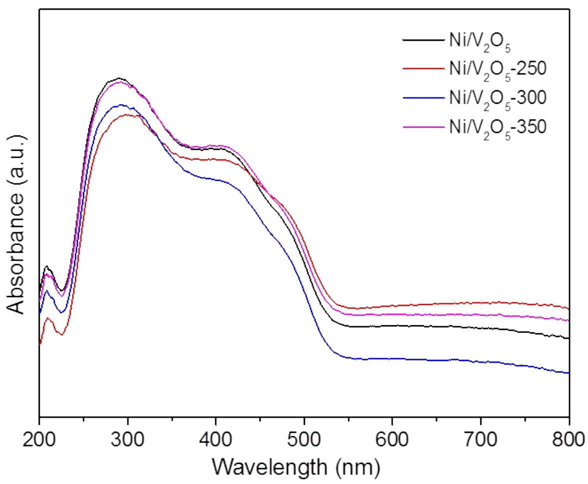


**Fig. S23** UV-vis spectra of four Ni-based catalysts.

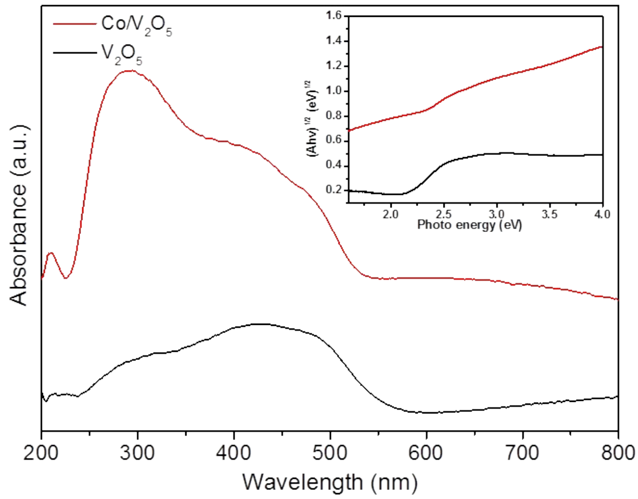


**Fig. S24** UV-vis spectra and the plots of the $(Ahv)^{1/2}$ vs photon energy of $V_2O_5$ and Co/ $V_2O_5$.

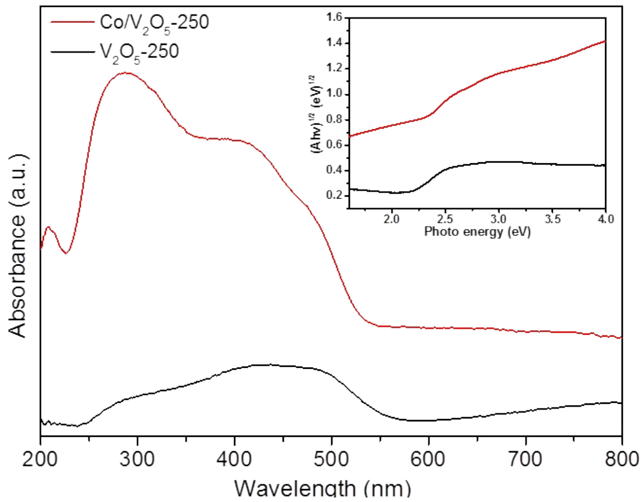


**Fig. S25** UV-vis spectra and the plots of the $(Ahv)^{1/2}$ vs photon energy of $V_2O_5$-250 and Co/ $V_2O_5$-250.

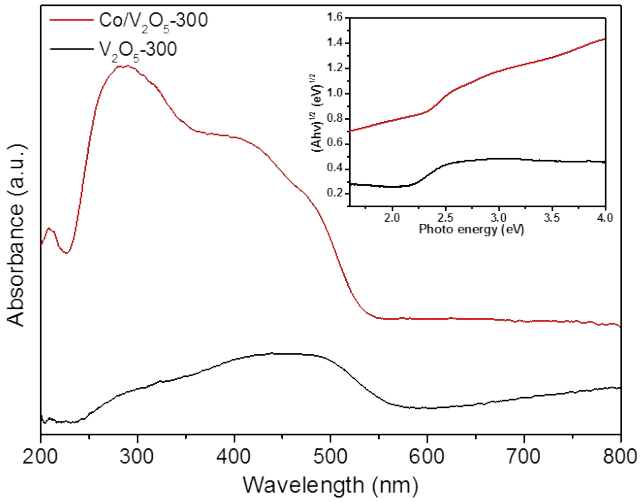


**Fig. S26** UV-vis spectra and the plots of the $(Ahv)^{1/2}$ vs photon energy of $V_2O_5$-300 and Co/ $V_2O_5$-300.

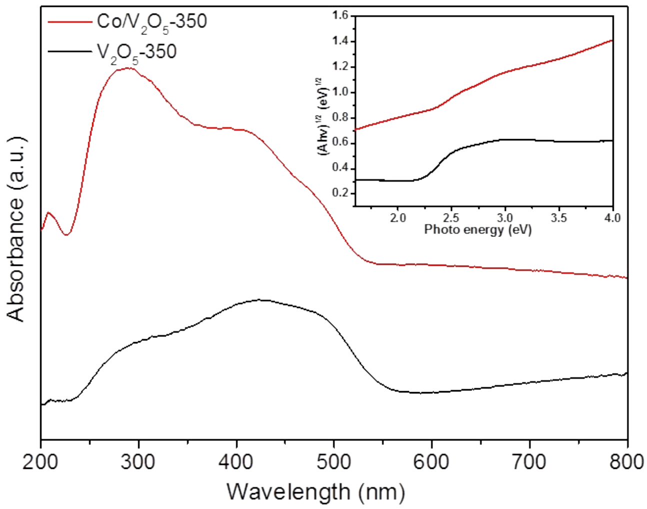


**Fig. S27** UV-vis spectra and the plots of the $(Ahv)^{1/2}$ vs photon energy of $V_2O_5$ and Co/ $V_2O_5$.

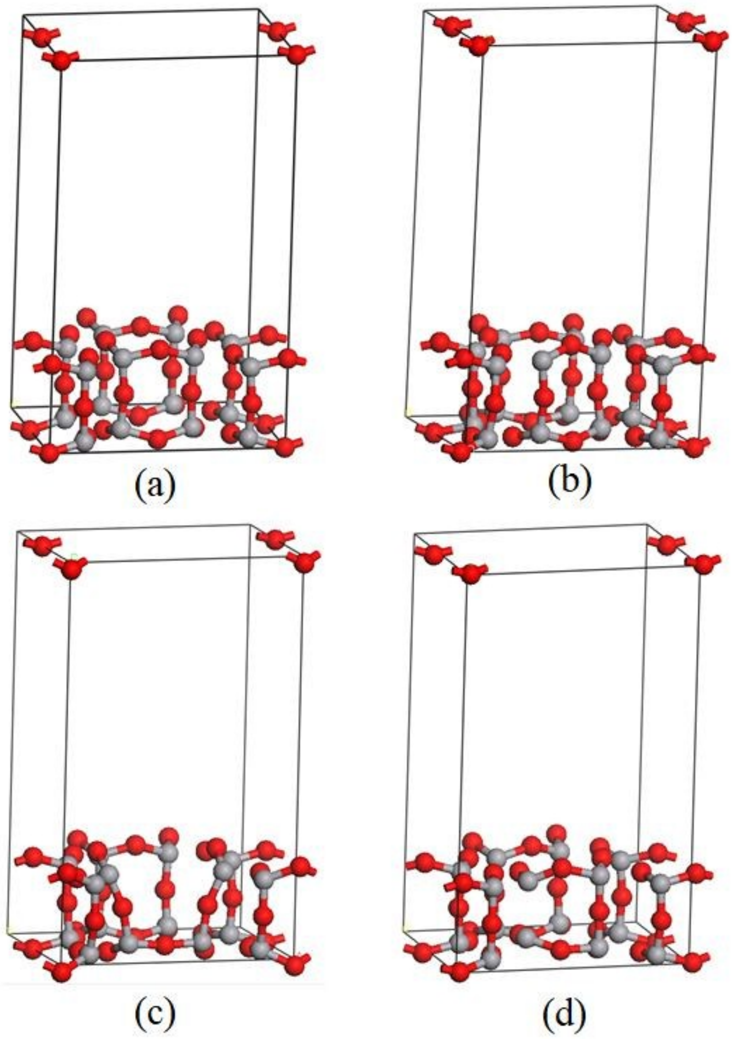


**Fig. S28** Supercell models proposed for (a) pristine $V_2O_5$, (b) $V_2O_5$ with double vanadyl bond oxygen vacancy, (c) $V_2O_5$ with bridging oxygen vacancy and (d) triple bonding oxygen vacancy.

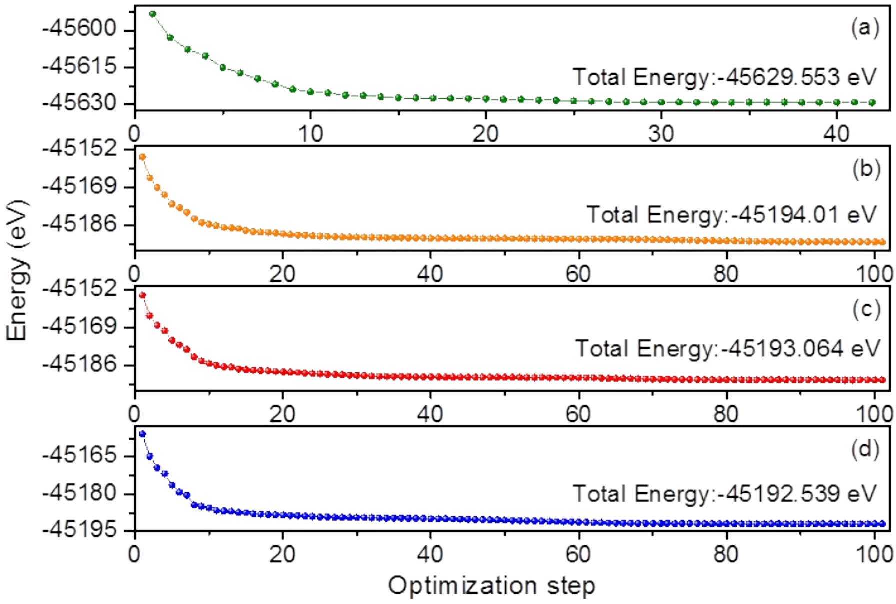


**Fig. S29** Total energy and energetic convergence data of all calculated models: (a) pristine $V_2O_5$, (b) $V_2O_5$ with double vanadyl bond oxygen vacancy, (c) $V_2O_5$ with bridging oxygen vacancy and (d) triple bonding oxygen vacancy.

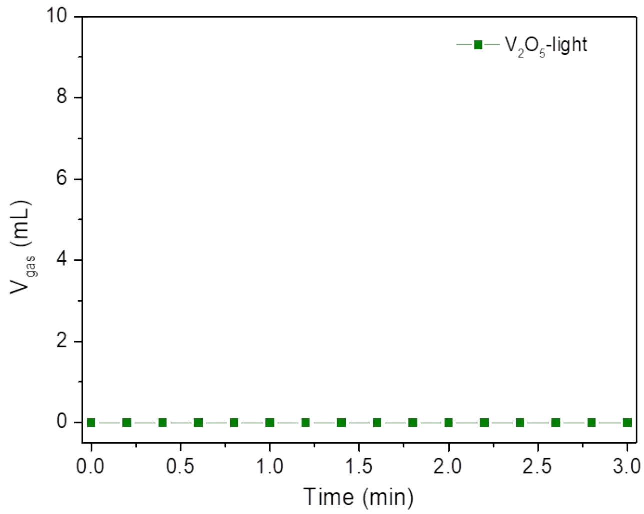


**Fig. S30** Plots of time versus volume of $H_2$ evolution from $NH_3BH_3$ aqueous solution over $V_2O_5$.

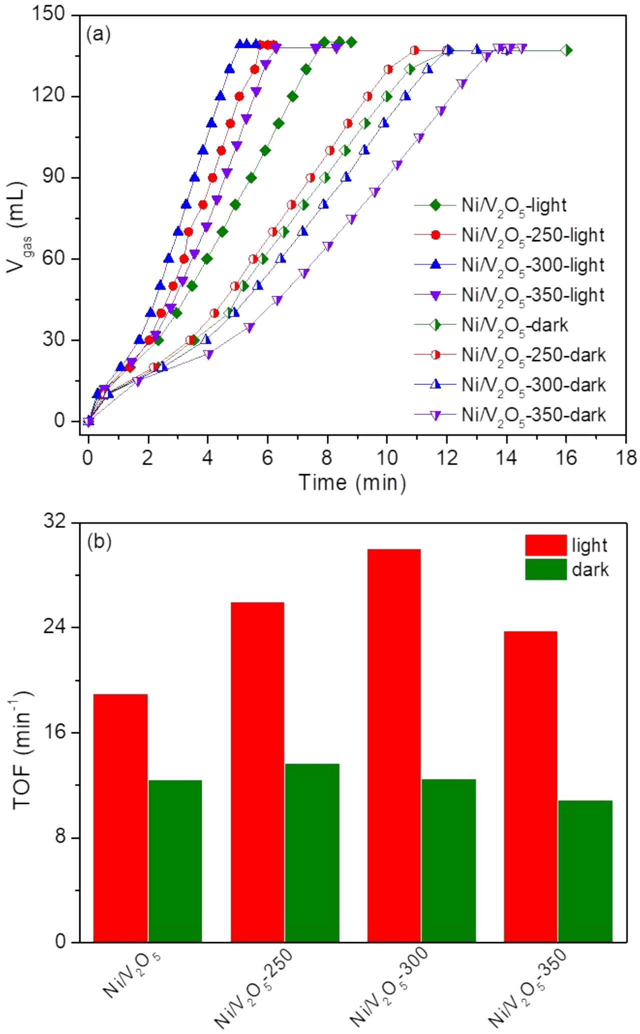


**Fig. S31** Plots of time versus volume of $H_2$ evolution from $NH_3BH_3$ in the aqueous solution over four Ni-based catalysts under visible light irradiation and in the dark and (b) the total TOF values.

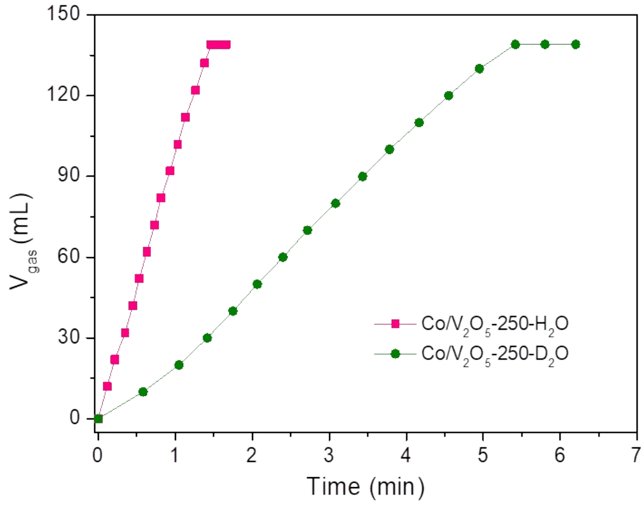


**Fig. S32** Plots of time versus volume of $H_2$ evolution from $NH_3BH_3$ in $H_2O$ or $D_2O$ over $Co/V_2O_5$-250 under visible light irradiation.

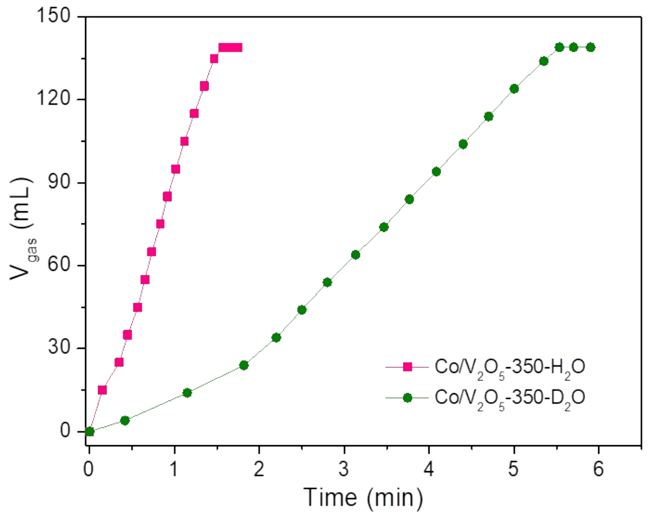


**Fig. S33** Plots of time versus volume of $H_2$ evolution from $NH_3BH_3$ in $H_2O$ or $D_2O$ over $Co/V_2O_5$-350 under visible light irradiation.

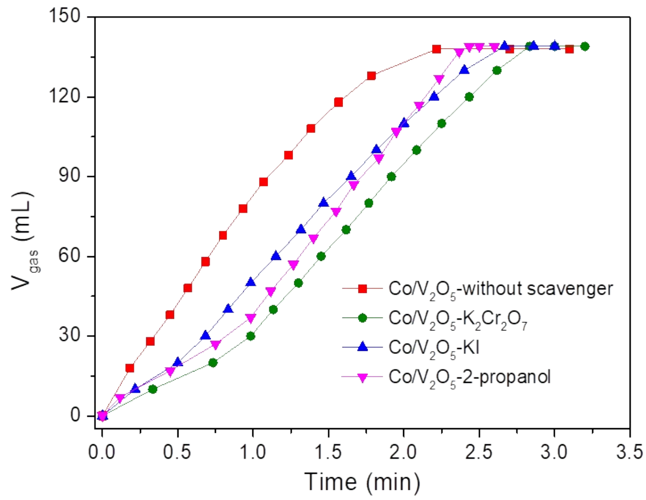


**Fig. S34** Time versus volume of $H_2$ evolution from $NH_3BH_3$ in the alkaline aqueous solution over Co/$V_2O_5$ without scavenger or in the presence of 2-propanol, $K_2Cr_2O_7$ and KI under visible light irradiation.

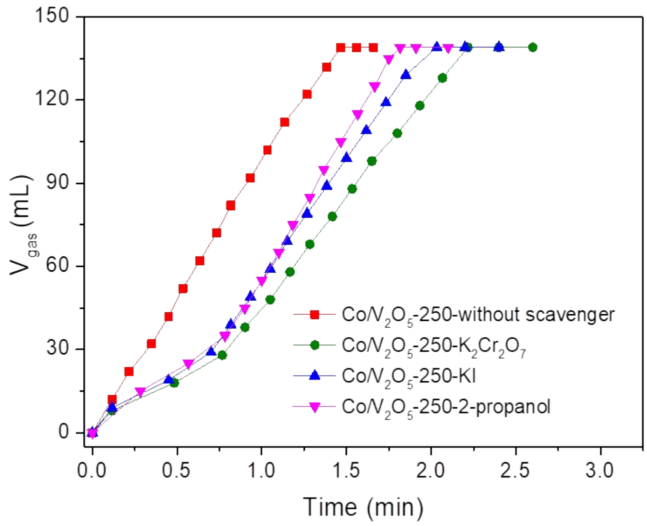


**Fig. S35** Time versus volume of $H_2$ evolution from $NH_3BH_3$ in the alkaline aqueous solution over Co/$V_2O_5$-250 without scavenger or in the presence of 2-propanol, $K_2Cr_2O_7$ and KI under visible light irradiation.

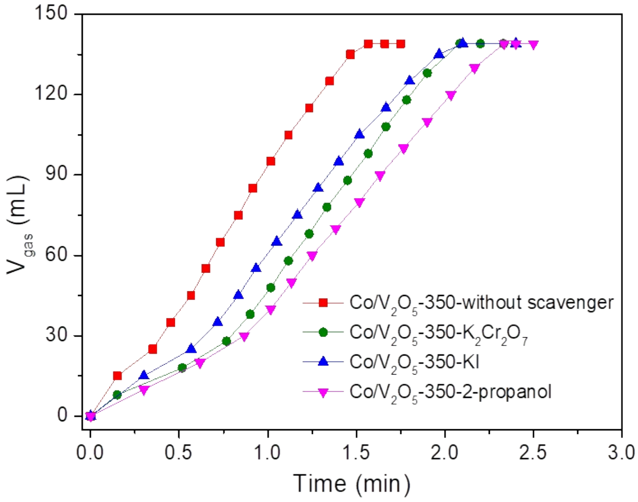


**Fig. S36** Time versus volume of $H_2$ evolution from $NH_3BH_3$ in the alkaline aqueous solution over Co/$V_2O_5$-350 without scavenger or in the presence of 2-propanol, $K_2Cr_2O_7$ and KI under visible light irradiation.